Quantum mechanically complete measurements in electron impact excitation of helium

Andrew G. Mikosza

Centre for Atomic, Molecular and Surface Physics,
Physics Department, The University of Western Australia,
Nedlands, Perth. 6907, Australia.

Abstract. A complete quantum description of the 3^1D state of helium, that is the amplitudes and relative phases for the m = 0, ±2 magnetic sublevels are reported. All state multipoles $\langle T(2)_{kq} \rangle$ ($k = 0$–4, $k \geq q \geq -k$) that describe the population and the anisotropy of the excited He(3^1D) state are presented. The data were determined for 60eV incident electrons and 40° electron scattering angle.

The experimental procedure was to measure the triple-coincidence, polarisation correlations of the sequential cascading photons (667.8 nm $3^1D \rightarrow 2^1P$ and 58.4 nm $2^1P \rightarrow 1^1S$ transitions) and the scattered n = 3 energy loss electrons. Simultaneous measurements of the three two-particle coincidence pairs determined accurate magnitudes of the scattering amplitudes and phases as well as enabling consistency checks with earlier data. The triple coincidence data determined the sign of the relative m = ±2 phases. The results are presented in a simplifying diagrammatic form. As yet there are no other complete experimental determinations of the 3^1D state.

The measurements are in agreement, within the experimental uncertainty, with the Convergent Close Coupling (CCC) calculations.

Previous data for helium at 40eV incident electrons are discussed in the context of the present triple-coincidence results. The desirability of a recently introduced parameter notation for the helium $3^{1,3}D$ states is questioned with respect to physical insight.

INTRODUCTION

The experimental and theoretical investigations of electron collisions with atoms leads to a better understanding of atomic structure, particle interactions and collision processes. Here we are concerned with electron impact excitation of helium for which the structure and interactions are well known and the fundamental information to be obtained is the scattering amplitudes and their relative phases. From those quantities the data of differential and total scattering cross sections can be calculated for applications in, for example, astrophysics, stellar and planetary atmospheres, laser physics and plasma physics.

Although there is at present a considerable interest in quantum mechanically complete description of an atomic states, experimentally the goal has only been

CP500, *The Physics of Electronic and Atomic Collisions*, edited by Y. Itikawa, et al.

attained for the 2^1P and 3^1P states of helium. Reviews have been given by, for example, Andersen and Bartschat (1) and Andersen (2,3).

The necessary set of measurements for these P states has been obtained for electron impact through measurements of coincident pairs of scattered electrons and radiated photons emitted after the excitation process.

Earlier studies of the 3^1D excitation process made observations in the scattering plane, defined by the incident and scattered electron momentum vectors, of scattered pairs of particles and observed either angular or polarisation correlations. Andersen and Bartschat (4) have also reviewed electron impact excitation of D states of atoms, pointing out that after the work in the early 1980's (5-7) on the D state excitation, it became clear that a scattered particle and one photon coincidence experiments would not allow a unique determination of all the complex scattering amplitudes.

In this paper we extend the complete quantum mechanical description to the 3^1D state of helium with measurements of triple coincidence observations of the scattered electron and two photons (D $\rightarrow$ P followed by P $\rightarrow$ S). The most recent studies on the D state are discussed first.

THE HELIUM 3^1D STATE AND COMPLETE EXPERIMENTS

The coincidence detection of the energy loss electron and the cascade 58.4 nm $2^1P \rightarrow 1^1S$ photon enabled the determination of the polarisation anisotropy parameters λ, $|\chi|$, $|\mu|$ and η defined by van Linden van Den Heuvell *et al.* (6). The only other angular correlation measurement, by Perera and Burns (8), observed the 667.8 nm $3^1D \rightarrow 2^1P$ photons in coincidence with the energy loss electron. They expressed their results in terms of γ_a, P_{lin}, ρ_{oo}

Further coincidence measurements of the scattered energy loss electron and the 667.8 nm photon used polarisation correlations, in the direction perpendicular to the scattering plane, to obtain the Stokes parameters P_i (i=1-3) and hence the γ, P_ℓ and $L_\perp$ parameters (9-11).

More detailed measurements included the determination of Stokes parameter P_4 by measurements in-the-scattering plane of polarisation correlations and hence the electron charge cloud height parameter ρ_{oo} (12-14).

Coincidences between the sequential cascading photons, with polarisation analysis of the first photon (15,16), enabled the first determination of a rank four, zero order, state multipole for the 3^1D state, and of the total (integrated over scattered electron angle) magnetic sublevel cross sections for m = 0, 1 and 2 separately.

The above experimental results for the 3^1D state may be compared in terms of the fundamental scattering amplitudes and phases, the Stokes parameter measurements, and also in terms of the state multipoles. These comparisons, shown in table 1, highlight the missing information required for a complete description of the helium D state.

TABLE 1. Selected experimental work leading up to the full description of the He(3^1D).

Selected experimental work on He(3^1D)	Scattering Amplitudes and Phases [a]	Target / coherence parameters [a]	Stokes Parameters	State Multipoles $\langle T(L_2)_{kq} \rangle$
van Linden van Den Heuvell *et al.* (1983)	$\lvert\alpha_0\rvert^2$, $\alpha^*_{+2}+\alpha_{-2}$	γ_a, P_{lin}, ρ_{00}	P_1, P_2, P_4	$k = 0, 2$ $q = 0$
Beijers *et al.* 1987	$\alpha^*_{+2}+\alpha_{-2}$	γ_a, P_{lin}, $(L_\perp = -\sqrt{1-P^2_{lin}})$	P_1, P_2 $(P_3 = \sqrt{1-P^2_{lin}})$	$k = 0, 2$ $q = 0$
Batelaan *et al.* 1988	α_{+2}, α_{-2}, $\alpha^*_{+2}+\alpha_{-2}$	γ_a, $L_\perp$, P_{lin}	P_1, P_2, P_3	$k = 0, 1$ $q = 0$
Donnelly and Crowe 1988	α_{+2}, α_{-2}, $\alpha^*_{+2}+\alpha_{-2}$	γ_a, $L_\perp$, P_{lin}	P_1, P_2, P_3	$k = 0, 1$ $q = 0$
Perera and Burns 1990	$\lvert\alpha_0\rvert^2$, $\alpha^*_{+2}+\alpha_{-2}$	γ_a, P_{lin}, ρ_{00}	P_1, P_2, P_4	$k = 0, 2$ $q = 0$
Batelaan *et al.*, 1991	α_0, α_{+2}, α_{-2}, $\alpha^*_{+2}+\alpha_{-2}$	γ_a, $L_\perp$, P_{lin}, ρ_{00}	P_1, P_2, P_3, P_4	$k = 0-2$ $q = 0-2$
Mikosza *et al.*, 1994	α_0, α_{+2}, α_{-2}, $\alpha^*_{+2}+\alpha_{-2}$	γ_a, $L_\perp$, P_{lin}, ρ_{00}	P_1, P_2, P_3, P_4	$k = 0-2$ $q = 0-2$
Donnelly *et al.*, 1994	α_0, α_{+2}, α_{-2}, $\alpha^*_{+2}+\alpha_{-2}$	γ_a, $L_\perp$, P_{lin}, ρ_{00}	P_1, P_2, P_3, P_4	$k = 0-2$ $q = 0-2$
Mikosza *et al.*, 1995	$\lvert\alpha_0\rvert^2$, $\lvert\alpha_{+2}\rvert^2$, $\lvert\alpha_{-2}\rvert^2$	ρ_{00}, σ_1, σ_2, σ_3	P_1, P_4 $(P_2 = P_3 = 0)$	$k = 0-4$ $q = 0$
Complete description (present work)	α_0, α_{+2}, α_{-2} $(\beta_{+2})_0$, $(\beta_{-2})_0$	γ_a, $L_\perp$, P_{lin}, ρ_{00} $\gamma^\pm_a$, $L^\pm_\perp$, $P^\pm_{lin}$, $\rho^\pm_{00}$ [b]	P_1, P_2, P_3, P_4 $(P_1)^{triple}$, $(P_2)^{triple}$	$k = 0-4$ $q = 0-4$

[a] The parameters γ_a, $L_\perp$, P_{lin}, ρ_{00} or α_0, α_{+2}, α_{-2}, and $\alpha^*_{+2}+\alpha_{-2}$ do not allow a unique determination of the 3^1D state.

[b] Parameters with the indicated (±) separate values are obtained from the D state decay channels via the m = ± 1 magnetic sublevels.

An analysis of the decay of excited D-state atoms is based on Fano and Macek (17), Blum and Kleinpoppen (18), Blum (19), Heck and Gauntlett (20) and Wang *et al.* (21). The present work (last row in the above table), is the first complete description of the 3^1D state obtained from the triple coincidence observation of the scattered energy loss electron and the two sequential cascading photons. In the experimental setup, where the first photon polarisation and the second photon intensity (without polarisation) were measured in coincidence, the Stokes parameters are given by, (21)

$$IP_1 = -\sum_{\lambda_1=\dot{\lambda}_1=\pm 1}[\rho(\lambda_2=-1;\dot{\lambda}_2=1)+\rho(\lambda_2=1;\dot{\lambda}_2=-1)],$$

$$IP_2 = i \sum_{\lambda_1=\lambda_1'=\pm 1} [\rho(\lambda_2 = -1; \lambda_2' = 1) - \rho(\lambda_2 = 1; \lambda_2' = -1)] \quad \text{and}$$

$$IP_3 = \sum_{\lambda_1=\lambda_1'=\pm 1} [\rho(\lambda_2 = 1; \lambda_2' = 1) - \rho(\lambda_2 = -1; \lambda_2' = -1)] \qquad (1)$$

The Stokes parameters obtained from these three particle polarisation correlations measurements are related to the D state multipoles $\langle T(L_2)^{\dagger}_{kq} \rangle$, with rank k and order q up to 4 by, (22)

$$IP_i = \mathrm{C} \sum_{kq} IPi[k,q] \langle T(L_2)^{\dagger}_{kq} \rangle_{lab} \qquad (\text{for } i = 1,2,3)$$

The rank 4 state multipoles describe the population and the anisotropy of the excited He(3^1D) state fully.

A description of the experimental method follows, together with the information that can be obtained obtained, firstly from the simultaneous observation of two-particle coincidences and then from observations of three-particle coincidences.

EXPERIMENTAL ASPECTS

The experimental method, schematically indicated in figure 1, involves electron impact excitation of helium atoms and the triple coincident detection of the energy loss electron and the two sequential cascade photons following the decay of the excited 3^1D state via the intermediate 2^1P to the 1^1S ground state. The apparatus is a crossed electron and atomic beams system, which has been described in detail previously (23).

Briefly it consists of a cylindrical vacuum chamber with rotatable electron gun, electrostatic 180° electron energy analyser, and an in-the-scattering-plane vacuum ultraviolet (VUV) photon detector. The helium target gas effused from a single capillary with 0.3 mm diameter and 5 mm length located on the central axis of the rotary tables, with typical driving pressures behind the capillary were 0.2–0.5 Torr resulting in a background pressure of about 1×10^{-7} Torr. This pressure was low enough for pressure-dependent effects, due to resonance trapping arising from the absorption and subsequent re-emission of the emitted $2^1\mathrm{P} \rightarrow 1^1\mathrm{S}$ (58.4 nm) photons, to be negligible for the present measurements.

The first (visible) photon (γ_1) originates from the $3^1\mathrm{D} \rightarrow 2^1\mathrm{P}$ transition at 667.8 nm. These photons were selected by a cone with entrance solid angle of 85 degrees, followed by a lens to form a parallel beam which was subsequently passed through the appropriate 'retarder and linear polarizer combination' to permit a full polarization analysis. Two different visible polarizer/detector systems were used to view the

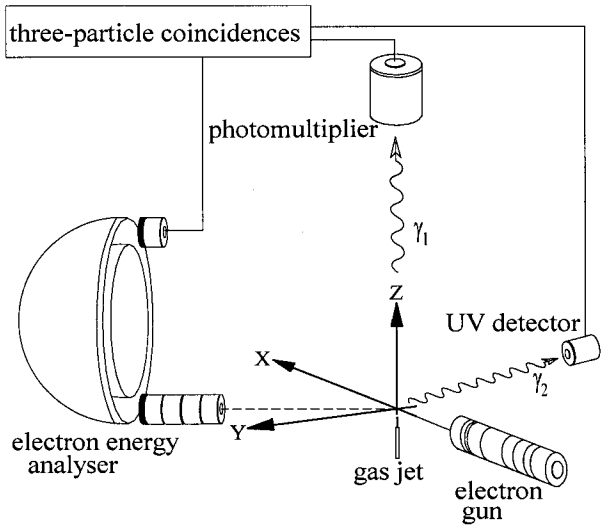

FIGURE 1. A schematic of the apparatuss and geometry for three-particle coincidence measurements.

collision region perpendicular to the electron beam direction in either perpendicular (vertical) or parallel (horizontal), respectively, to the collision plane.

All (visible and VUV) photons were detected perpendicular to the electron beam ($\theta_1 = \theta_2 = 90°$). The relative (azimuthal) angle $\Delta\phi = \phi_1 - \phi_2$ between the visible (γ_1) and the VUV (γ_2) photon was chosen as $\Delta\phi = 90°$ and $\Delta\phi = 180°$ for the vertical and horizontal visible photon detection systems, respectively.

The signals from the scattered electron (e^-), the visible photon (γ_1) and the cascade UV photon (γ_2) were used to start and stop two TACs resulting in three types of output. The first type are the three-particle coincidence counts with the scattered electron and the two photons originating from the same helium atom (e^-, γ_1, γ_2). The second type originates from the three possible ways in which two of the three signals are correlated, (e^-, γ_1), (e^-, γ_2) and (γ_1, γ_2), with the third signal γ_2 , γ_1 and e^- respectively, accidental. These three two-particle correlated contributions to the overall counts represent the accidental coincidences in triple coincidence measurements. The third type of output is the totally accidental contribution with all three, e^-, γ_1 and γ_2 , uncorrelated.

These types of output signals, and their low coincidence count rates, required the development and optimisation of a computer controlled interactive real-time data acquisition, analysis and display system (24). The system is capable of uniquely identifying the three-particle, the two-particle coincidences and the totally accidental counts from the three detectors.

To describe the excited 3^1D state fully, we employed our three-particle coincidences detection simultaneously with the most common experimental approach used on the 3^1D state, the two-particle polarization correlations detection. From these polarization

correlations measurements of the first cascade photon and the scattered electron, with the visible light analysis perpendicular to the scattering plane, we obtained the Stokes parameters P_i (i = 1-3). Further polarization correlations measurements with in-the-scattering-plane analysis of the visible light provided the P_4 Stokes parameter. The Stokes parameter values for P_i (i = 1, 2 and 4) were obtained concurrently with the three-particle, P_1^t and P_2^t, coincidences Stokes parameter measurements, and the Stokes parameter P_3 subsequently, using a suitable retarder.

The three and two-particle coincidences were accumulated simultaneously for other reasons also. The accumulated data enabled consistency checks to be made of the deduced scattering amplitudes and phases of earlier data and to obtain the present amplitude data with decreased experimental uncertainties. The latter was made possible by the long three-particle coincidences accumulation times.

RESULTS

Two-particle coincidence experiments

In the natural coordinate frame and with negative reflection symmetry, the m = ± 1 states are not populated. With one arbitrary phase and normalisation to the differential cross section for exciting the 3^1D state, there are only four independent parameters to be determined, namely the two m = ± 2 amplitudes, $\alpha_{\pm 2}$, and their phases, $\beta_{\pm 2}$, with respect to the α_0 amplitude (25). In the present study using the double coincidence electron-photon polarization correlation experimental method, in which polarization analysis is made only of the $3^1\mathrm{D} \rightarrow 2^1\mathrm{P}$ 667.8 nm photons, the scattering amplitudes are related to the Stokes parameters by

$$I_{in-plane} = \frac{2}{3}\alpha_0^2 = (1-P_1)\,(1-P_4)/[4-(1-P_1)\,(1-P_4)] \tag{2}$$

$$I_z P_3 = -(\alpha_{+2}^2 - \alpha_{-2}^2) \tag{3}$$

$$I_z = \alpha_{+2}^2 + \alpha_{-2}^2 + \frac{1}{3}\alpha_0^2 \tag{4}$$

$$I_z P_1 = -\sqrt{\tfrac{2}{3}}\,\alpha_0(\alpha_{+2}\cos\beta_{+2} + \alpha_{-2}\cos\beta_{-2}) \tag{5}$$

$$I_z P_2 = -\sqrt{\tfrac{2}{3}}\,\alpha_0(-\alpha_{+2}\sin\beta_{+2} + \alpha_{-2}\sin\beta_{-2}), \tag{6}$$

where polarization analysis of the visible light intensity in the z-direction, I_z, perpendicular to the scattering plane determines P_1, P_2 and P_3. In-the-scattering plane linear polarization analysis determines P_4. The values of α_0, α_{+2} and α_{-2} are then obtained from equations (2) to (4). Polarization correlations measurements of P_1 and P_2, equations (5) and (6) determine the phases β_{+2} and β_{-2}, but not the relative phase between β_{+2} and β_{-2}, with the consequence that the corresponding amplitude sum can be obtained by two alternative phase combinations; the 'real' and the 'ghost' solutions, that are indistinguishable in two particle-coincidence experiments.

The two solutions for the amplitude (vector) sum $\alpha_{+2} + \alpha_{-2}$ are best described by the alternative phases (β^{I}_{+2} and β^{II}_{+2}) and (β^{I}_{-2} and β^{II}_{-2}), and our present results are shown in table 2. With the stated aim of describing the 3^1D state fully, table 2 also lists all the other results that can be obtained using the two-particle coincidence, polarization correlation experimental method, that does not identify the 'real' solution. For example, the derived atomic properties of the charge cloud, namely the linear polarization P_{lin}, the alignment of the charge cloud γ, the angular momentum L and the height of the charge cloud (ρ_{oo}), are identical for the two solutions.

The two-particle coincidence results, obtained with 60eV electron impact energy and 40° electron scattering angle, represent the 'first step' towards the full description of the 3^1D state. The final and 'second step', which can only be provided by the more difficult three-particle coincidence measurements, allows the identification of the 'real' solution.

However before the three-particle coincidence results are presented and the identification of the real solution is made, it is instructive to illustrate diagramatically the alternative solutions provided by the two-particle coincidence polarization

TABLE 2. The 3^1D parameters obtained from polarization correlations (e^-, γ e^-) experiments, with 60eV energy electron impact electrons and 40° scattering angle. The right hand side columns show the alternative phases β^{I}_{+2} or β^{II}_{+2}, and β^{I}_{-2} or β^{II}_{-2}, for the α_{+2} and α_{-2} amplitudes, respectively. The values of P_i (i = 1, 2, 3 and 4) agree well with our previous polarization correlations experiments (13).

Stokes Parameters		**Charge Cloud Parameters**		**Scattering Amplitudes**		**Alternative Phases**	
P_1	0.424 ± 0.049	P_{lin}	0.427 ± 0.049	α_{+2}	0.513 ± 0.043	β^{I}_{+2}	−150.0° ± 14.2°
P_2	−0.047 ± 0.060	γ_a	−3.16° ± 4.02°			β^{II}_{+2}	−197.4° ± 14.2°
P_3	− 0.375 ± 0.040	L	0.410 ± 0.101	α_{-2}	0.240 ± 0.027	β^{I}_{-2}	294.4° ± 37.8°
P_4	− 0.075 ± 0.086	ρ_{oo}	0.679 ± 0.066			β^{II}_{-2}	52.9° ± 37.8°
				α_0	0.824 ± 0.066		

correlations experiments. Briefly, for the selected geometry and polarisation correlation approach mentioned above, the measured two and three-particle coincidence Stokes parameters are directly related to the excitation amplitudes and their phases by equation (1). The limitations of the amplitude information obtainable in the two-particle coincidence case (equations (5) and (6)), the result of summing equation (1) over all angles of the undetected second cascade photon, are most apparent from the alternative phases for α_{+2}, and α_{-2} in table 2, and from figure 2. Figure 2 clearly shows the amplitude vector sum $\alpha_{+2}^{*} + \alpha_{-2}$ together with the two possible solutions, and the angular values of the alternative phases $-\beta_{+2}^{I}$ or $-\beta_{+2}^{II}$ and β_{-2}^{I} or β_{-2}^{II}, for α_{+2}^{*} and α_{-2}, respectively. The diagram also shows the electron space charge alignment angle γ_a, for our chosen electron scattering angle. The choice of the 40° scattering angle is crucial, and can be seen from our previous measurements (13) of two-particle coincidences at the scattering angles of 15° and 25°, shown in figure 3. The experimental uncertainties for these solutions overlap and are significantly larger than the uncertainties of the present results at the electron scattering angle of 40°. The reduced experimental uncertainties for the 40° data reflect that a much larger data accumulation time, as well as apparatus improvements, for these measurements. The symbols at 15° and 25° indicate paired real and ghost solutions since they have not yet been identified. It can be seen that at 40° electron scattering angle the real and ghost solutions diverge, allowing easier identification of the real solution from the three particle coincidence results. Also, it is easy to deduce the statistical accuracy needed for both two and three-particle coincidence measurements of specific relative phases in order for the present approach to be successful in separating the real and ghost phases. The more difficult three-particle coincidence measurements were used only to identify the real solution. The statistically more accurate two-particle coincidence measurements provided all of the necessary excitation amplitudes data apart from the relative phase of $\beta_{\pm 2}$.

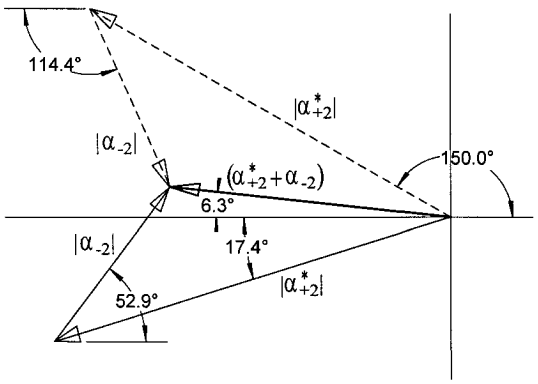

FIGURE 2. The vector sum $\alpha_{+2}^{*} + \alpha_{-2}$ together with the two possible solutions (see text).

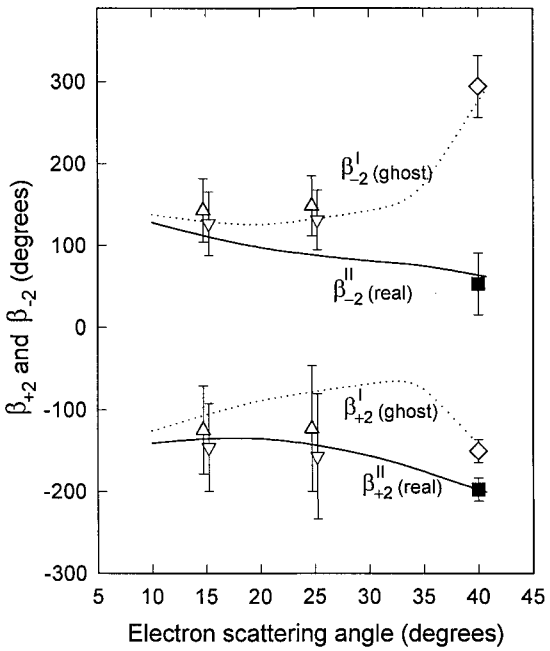

FIGURE 3. The relative phases, β_{+2} and β_{-2}, of the amplitudes α_{+2} and α_{-2}, respectively, as a function of the electron scattering angle. The two-particle (e^-,γ_1) coincidence measurements (13) provide the possible real β^{I} (∇) and ghost β (Δ) values. At 40^0 scattering angle, the two-particle coincidence data, obtained concurrently with three-particle coincidence measurements, are identified as the real β^{I} (■) and as the ghost β ($\Diamond$) solutions (see Three-partile Coincidence Experiments section). The convergent close coupling (CCC) phases (27) are shown as the full lines, while the inferred CCC ghost values are the dotted lines.

Figure 3 showing the alternative ($\beta_{\pm2}$) phases is preferred to the equivalent $\gamma^{\pm}$ plots for the excited D state (4), where the ± separate values are obtained from decay channels via the m = ± 1 magnetic sublevels. Also the real and ghost solutions are more clearly represented by vector diagrams as in figure 2 than by $\gamma^{\pm}$ triangles (25), in particular when errors determine triangle closures.

The real and the ghost solutions can also be shown schematically, in the atomic scattering reference frame ($\gamma_a = 0$), by the two 3^1D electron charge cloud distributions (figure 4 (top)), given by the angular part of the electron charge density equation (26),

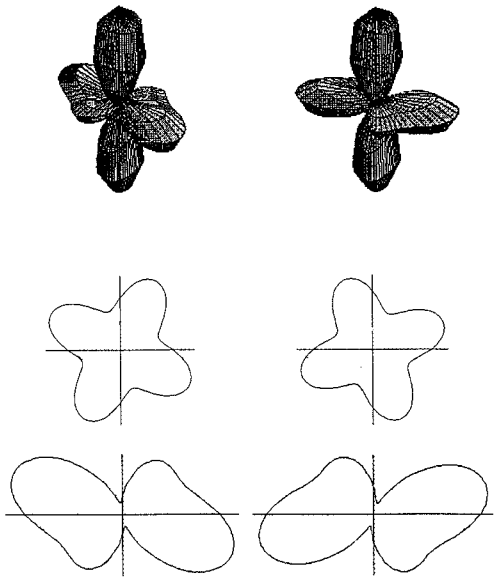

FIGURE 4. The real and the ghost solutions of the He(3^1D) state excited by 60eV energy electron impact electrons, at 40^0 electron scattering angle (see text).

$$
\begin{aligned}
Y^a(\theta,\phi) &= (\alpha_2^2 + \alpha_{-2}^2)\tfrac{3}{8}\sin^4\theta + \alpha_0^2\,\tfrac{1}{4}(3\cos^2\theta - 1)^2 \\
&\quad - P_{lin}(\alpha_2^2 + \alpha_{-2}^2 + \tfrac{1}{3}\alpha_0^2)\tfrac{3}{4}\sin^2\theta(3\cos^2\theta - 1)\cos 2\phi \\
&\quad + \alpha_2\alpha_{-2}\,\tfrac{3}{4}\sin^4\theta\cos 4(\phi - \eta) \\
&= A_0(\theta) + A_2(\theta)\cos 2\phi + A_4\cos 4(\phi - \eta),
\end{aligned}
$$

where $\eta = (\beta_{-2} - \beta_2)/4$. The difference between the real and ghost charge clouds is the sign of η. The two possible solutions for the sum $\alpha_{+2}^* + \alpha_{-2}$, are now represented by the undetermined sign of the third term of the equation. If the charge cloud is separated into its components, the asymmetric contribution of the third term, together with the isotropic first term, is shown in figure 4 (middle) projection onto the X-Y plane. As a result the complete ghost and the real charge clouds display a reflection symmetry about the X-Z plane, in the atomic scattering reference frame, as shown in figure 4 (bottom) projections onto the X-Y plane. The two charge clouds are indistinguishable by any of the parameters, α_{-2}, α_0, α_{+2}, γ_a, L , P_{lin}, ρ_{oo}, P_1, P_2, P_3, P_4; only the relative phase difference ($\beta_{+2} - \beta_{-2}$), if known, will distinguish the 'real' from the 'ghost' distribution.

Three-particle coincidence experiments

The double coincidence correlations measurements of P_1 and P_2, have determined the phases β_{+2} and β_{-2} but not their relative phase as indicated by the two possible solutions to the vector sum $\alpha_{+2}^{*} + \alpha$.

The determination of the relative phase requires interference between the scattering amplitudes α_{+2} and α_{-2} and necessitates triple coincidence measurements. In our experimental geometry the visible photon detector is located perpendicular to the scattering plane, the UV detector is in the scattering plane and both detectors are at 90 degrees to the incident electron beam. Then the triple coincidence intensity and polarisations of the visible photon perpendicular to the scattering plane in the natural reference frame are given by

$$I_z^t = \tfrac{1}{6}\alpha_0^2 + \tfrac{1}{2}(\alpha_{+2}^2 + \alpha_{-2}^2) - \tfrac{1}{\sqrt{6}}\alpha_0(\alpha_{+2}\cos\beta_{+2} + \alpha_{-2}\cos\beta_{-2}) \quad (7)$$

$$I_z^t P_1^t = \tfrac{1}{6}\alpha_0^2 - \tfrac{1}{\sqrt{6}}\alpha_0(\alpha_{+2}\cos\beta_{+2} + \alpha_{-2}\cos\beta_{-2}) + \alpha_{+2}\alpha_{-2}\cos(\beta_{+2} - \beta_{-2}) \quad (8)$$

$$I_z^t P_2^t = -\tfrac{1}{\sqrt{6}}\alpha_0(\alpha_{+2}\sin\beta_{+2} - \alpha_{-2}\sin\beta_{-2}) + \alpha_{+2}\alpha_{-2}\sin(\beta_{+2} - \beta_{-2}) \quad (9)$$

where the superscript indicates triple coincidence values. The relative phase difference $(\beta_{+2} - \beta_{-2})$, for the α_{+2} and α_{-2} amplitudes, is apparent in the cos and sin functions in equations 8 and 9, and hence the ambiguity inherent in the two particle coincidence polarization correlations experiments is resolved by measuring I_z^t, P_1^t and P_2^t. It is noted that there is no requirement to measure *both* of the three particle coincidence Stokes parameters P_1^t and P_2^t for the relative phase difference to be determined.

The measured values for the triple coincidence Stokes parameters are $P_1^t = 0.436 \pm 0.349$ and $P_2^t = 0.285 \pm 0.376$. Now, rather than solve equations 8 and 9 to determine β_{+2} and β_{-2}, we choose to (i) use the two phases determined from double coincidence measurements since they are considerably more accurate because the double coincidence count rates are about 10^3 times higher than the triple coincidence count rates and (ii) use the triple coincidence values of the Stokes parameters as limits for the true phases. The triple coincidence Stokes parameters which are implied by the two alternative values of the scattering amplitudes and phases of our $(e^-\gamma_1)$ polarization correlations experiments (table 2) are $P_1^t = 0.619$ and 0.482, and $P_2^t = -0.282$ and 0.330. The measured triple coincidence value of P_1^t of 0.436 ± 0.349 cannot separate the double coincidence values which both fall within the experimental uncertainty. However for P_2^t the determined $(e^-\gamma_1)$ value of -0.282 is outside the experimental

uncertainty of the triple coincidence measured value of 0.285 ± 0.376 hence it is the ghost solution. Therefore 0.330 is the *real* solution. This double coincidence real value of P_2^t was obtained using the β_{+2}^{II} (= −197.4°) and β_{-2}^{II} (= 52.9°) phases from the two possible solutions (table 2) scattering amplitudes α_{+2} and α_{-2}, respectively. Both the real and ghost double coincidence phases are shown in figure 2. The convergent close coupling (CCC) results (27) at 64.6 eV are P_1^t = 0.616 and P_2^t = 0.280 which are in agreement with the measured values within the experimental uncertainties.

The real and ghost value obtained with 60eV electron impact energy and 40° electron scattering angle, can be extended to nearby scattering angles and energies because of the monotonic variation of the phases with scattering angle and the similarity of figure 3 plots at energies close to 60eV.

Finally the state multipoles obtained from the two and three-particle results are shown, both in the natural and collision scattering frames.

TABLE 3. The state multipoles $\langle T(2)_{kq} \rangle$ (L=2) for the 3^1D state of helium excited by 60eV energy electrons and 40° scattering angle.

State Multipole	Collision frame	Natural frame
T_{00}	0.4471	0.4471
T_{1-1}	0.0919 i	0
T_{10}	0	0.1300
T_{11}	0.0919 i	0
T_{2-2}	0.1932	− 0.1518 + 0.0167 i
T_{2-1}	0.0167	0
T_{20}	− 0.0902	− 0.1915
T_{21}	− 0.0167	0
T_{22}	0.1932	− 0.1518 − 0.0167 i
T_{3-3}	**0.1900 i**	**0**
T_{3-2}	**− 0.2009 i**	**− 0.3696 − 0.2009 i**
T_{3-1}	**− 0.3203 i**	**0**
T_{30}	**0**	**0.0650**
T_{31}	**− 0.3203 i**	**0**
T_{32}	**0.2009 i**	**− 0.3696 + 0.2009 i**
T_{33}	**0.1900 i**	**0**
T_{4-4}	**0.1825**	**− 0.0415 − 0.1159 i**
T_{4-3}	**0.0274**	**0**
T_{4-2}	**0.3008**	**− 0.1315 + 0.0145 i**
T_{4-1}	**− 0.1136**	**0**
T_{40}	**0.2575**	**0.5253**
T_{41}	**0.1136**	**0**
T_{42}	**0.3008**	**− 0.1315 − 0.0145 i**
T_{43}	**− 0.0274**	**0**
T_{44}	**0.1825**	**− 0.0415 + 0.1159 i**

The additional state multipoles provided by the three-particle coincidence results are shown in bold.

CONCLUSIONS

In conclusion, the present the three-particle coincidence measurements have resolved the phase ambiguity of the less difficult two-particle coincidence (scattered electron and radiated photon) measurements of the excitation amplitudes and their phases for the 3^1D state of helium. A complete experiment for the 3^1D state of helium has been achieved. The real and ghost phases for other nearby energies and scattering angles can be inferred from the experimental results. The principle can be extended to higher-order coincidence measurements for higher angular momentum states.

REFERENCES

1. Andersen, N. and Bartschat, K., *Adv. At. Mol. Opt. Phys.* **36,** 1-85 (1996).
2. Andersen, N., Broad, J. T., Campbell, E. E. B., Gallagher, J. W., and Hertel, I. V., *Phys. Rep.* **278,** 107 (1997).
3. Andersen, N., Bartschat, K., Broad, J. T., and Hertel, I. V., *Phys. Rep.* **279,** 251 (1997).
4. Andersen, N. and Bartschat, K., *Adv. At. Mol. Opt. Phys.* **36,** 1 (1996).
5. Nienhus, G., *Coherence and Correlation in Atomic Collisions*, New York: Plenum, 1980, pp.121-32.
6. van Linden van Den Heuvell, H.B., van Gasteren, E.M., van Eck, J., and Heideman, H.G.M., *J. Phys B* **16**, 1619 (1983)..
7. Andersen, N., Gallagher, J. W., and Hertel, I. V., *Phys. Rep.* **165,** 1-188 (1988).
8. Perera, N.W.P.H., and Burns, D.J.J., *J. Phys B: At. Mol. Opt. Phys.* **23**, 3007 (1990).
9. Beijers, J.P.M., Doornenbal, S.J., van Eck and H.G.M. Heideman, J., *J. Phys B: At. Mol. Opt.* Phys. **20**, 6617 (1987).
10. Batelaan, H., van Eck, J., and Heideman, H.G.M., *J. Phys B* **21**, L741 (1988).
11. Donnelly, B.P., and Crowe, A., *J. Phys B* **21**, L637 (1988).
12. Batelaan, H., van Eck, J., and Heideman, H.G.M., *J. Phys B* **24**, L397 (1991).
13. Mikosza, A.G., Hippler, R., Wang, J.B., and Williams, J.F., *Zeit. Phys.* D **30**, 129 (1994).
14. Donnelly, B.P., McLaughlin, D.T., and Crowe, A., *J. Phys B: At. Mol. Opt. Phys.* **27**, 319 (1994).
15. Mikosza, A.G., Hippler, R., Wang, J.B., and Williams, J.F., *Phys. Rev. Lett.* **71** 235 (1993).
16. Mikosza, A.G., Hippler, R., Wang, J.B., and Williams, J.F. *Phys Rev. A* **53**, 3287-94 (1996).
17. Fano, U., and Macek, J.H., *Rev. Mod. Phys.* **45** 553 (1973).
18. Blum, K., and Kleinpoppen, H., *Phys. Rep.* **52** 203 (1979).
19. Blum, K., *Density Matrix Theory and its Application*, New York: Plenum Press, (1981).
20. Heck, E.I., and Gauntlett, J., *J. Phys. B* **19** 3633 (1986).
21. Wang, J.B., Williams, J.F., Stelbovics, A.T., Furst, J.E., and Madison, D.H., 1995 *Phys Rev A* **52,** 2885 (1995).
22. Wang, J.B., Stelbovics, A.T., and Williams J. F., *Zeit. Phys.* D **30**, 119-127 (1994).
23. Mikosza, A.G., Hippler, R., Wang, J.B., Williams, J.F., and Wedding, A.B., *J Phys B* **27**, 1429 (1994).
24. Mikosza, A.G., Williams, J.F., and Wang, J.B., *Phys. Rev. Lett.* **79** 3375-78 (1993).
25. Fursa, D.V., Bray, I., Donnelly, B.P., McLaughlin, D.T., and Crowe, A., *J Phys B* **30**, 3459 (1997).
26. Andersen, N., Gallagher, J.W., and Hertel, IV., *Phys. Rep.* **165,** 1 (1988).
27. Fursa, D.V., and Bray, I., *Phys. Rev. A* **52,** 2885 (1995), and private communication.